

GALACTIC AND SOLAR COSMIC RAYS

A. Chilingarian

Cosmic Ray Division, Yerevan Physics Institute, Alikhanian Brothers 2, Yerevan 36, Armenia.
chili@crdlx5.yerphi.am

Abstract

The aspects of Cosmic Ray (CR) origin are reviewed. Recent observational evidence on the spatial patterns of non-thermal X-ray radiation from Supernovae Remnants (SNR) support long waiting expectations of proton and nuclei acceleration up to PeV energies. We add new arguments based on the experimental data from surface arrays measuring Extensive Air Showers (EAS) and on data from solar accelerators available now from space born X-ray and gamma-ray spectrometers. Energy spectra of primary nuclei with atomic Number from from $Z=1$ to $Z=26$ can provide useful information on the validity of models of cosmic ray acceleration. By estimating the threshold energy of the onset of the suppression of the different nuclei flux, the so called spectral “knee” energy, we can directly check the hypothesis of rigidity dependent acceleration of the hadrons in SNR sites. Unfortunately, information from the EAS experiments does not provide enough clues for such “spectroscopy” of the “knee region.” Nonetheless, by grouping the primary nuclei in 2 or 3 broad mass groups (light, intermediate and heavy) we can obtain useful information on energy spectra of the primaries. Recently, using multidimensional classification methods on MAKET-ANI experimental data, we categorized the “all-particle” spectra into 2 distinct primary mass groups. From the spectra analysis, we come to the conclusion that the SNR based particle acceleration model is valid and presents evidence that there exists a nearby source of cosmic rays, which provides a significant portion of the CR flux.

INTRODUCTION

Cosmic Ray (CR) flux incident on terrestrial atmosphere consists mostly of protons and heavier stripped nuclei accelerated at numerous galactic and extragalactic sites. The most exciting question associated with cosmic rays is the exploration of a particular astrophysical accelerating source. Due to the bending in galactic magnetic fields, charged particles loose information about the parent sites during long travel and arrive to Earth highly isotropic. Only stable neutral particles i.e. X-ray, gamma quanta and neutrinos travel directly from sources and reveal exotic celestial objects and violent processes of their production. Orbiting telescopes and spectrometers, as well as, ground based Atmospheric Cherenkov Telescopes (ACT) and neutrino detectors have opened new windows to the Universe, detecting, in unprecedented details, the spreading of heavy elements during supernovae explosions, the ejection of the relativistic jets from black holes, and many other phenomena described in the last century only in science fiction.

A new paradigm in astrophysics research consists in the detection of celestial objects in radio, optical, X, and gamma rays. A variety of compatible measurements gives sufficient enough information for building realistic models of physical processes of supernovae explosions, of accompanying gamma-ray bursts, of accretion disc interactions with super-dense objects, and finally of the evolution of the Universe itself. In this case additional information about the particles of highest energies will significantly enlarge the information on the most violent processes in the Universe and on the processes of the largest particle accelerators in space.

Galactic cosmic rays cannot map the objects where they born, therefore, only integrated information from all sources are available from measurements of cosmic ray fluxes near Earth and on the

Earth's surface. This information consists of the shape of the energy spectra of the cosmic rays, their mass composition and their energy dependence, and of the anisotropy of the CR arrival.

Space-born spectrometers on the ACE satellite, the AMS detector on the Space Shuttle, as well as, numerous balloon-born detectors measure the fluxes of different isotopes up to energies of 10 TeV rather precisely. Particle fluxes follow an overall power-law of $I(E) \propto E^\gamma$ with spectral index of $\gamma \sim -2.7$. Therefore because of very the low fluxes of the highest energy CR's and due to very strict restrictions on the weight of the spacecraft payload, it is extremely difficult to get reliable information on particle fluxes above 10 TeV from space-born spectrometers and calorimeters. Although, it should be noted that recent successes with the long-lasting new technology balloon flights give hope that precise information on particle spectra up to several hundreds of TeV will be available soon.

Recently, the so called kinematical method (Adams et al., 2001) was proposed, using thin (about 10 g/cm^2) target and silicon coordinate and charge detectors to precisely detect the charge and emission angles of secondaries produced in an inelastic interaction of primary nuclei. The angle distribution of the particles produced in the target carry information about the energy of a primary particle. This technique does not require total release of the energy such as in the case of the ionization calorimeter and the instrument could be made very light in weight. A one-year flight of such a device on the Space Station will provide data up to several PeV with 0.2 units of charge resolution. Currently there is no funded space experiment in the PeV region and, at least in the current decade, data will only be accessible from the Extended Air Showers (EAS) initiated by the "primary" ion triggering a particle generation chain reaction in the terrestrial atmosphere and detected with large ground based particle detectors. A variety of physical processes during the travel of the relativistic cloud of "secondary" particles to the earth's surface gave rise to different experimental methods, aiming to reconstruct the particle type, trajectory, and energy.

Signatures of the primary particles are microwave radio signals, fluorescent light, cherenkov light, electrons, muons, neutrons, and hadrons reaching Earth's surface and muons detected deep underground. The intensity and correlation matrix of each combination of mentioned signals carry information on the primary particles, but due to the highly indirect nature of the experimentation, only some very robust characteristics of cosmic ray fluxes of PeV and higher energy primaries have been unambiguously established up to now. First of all it is all particle energy spectra, reconstructed from so-called size spectra measured by plastic or liquid scintillators (so called particle density detectors), distributed on the Earth surface. Assuming a definite shape of the EAS electron lateral distribution function, and measuring the density of electrons on some rectangular or circular grid of distributed density detectors, and using a standard minimization analysis technique, the overall number of electrons (shower size) can be determined. By measuring the time delay of the arriving of the shower particles, using a system of distributed "fast timing detectors", the zenith and azimuth angles of the shower core can be calculated (a very good estimate of the primary particle angles of incidence on the terrestrial atmosphere).

The shower size is correlated with the particle energy, but also with several unknown parameters such as particle type and the height of the first interaction. The functional form of the size-energy dependence introduces additional uncertainty, because it is obtained from a particular model of strong interaction of protons and ions with atmospheric nuclei, and at PeV energies there is no accelerator data to check this models. Different approximations of models fitted with manmade accelerator data at lower energies give significantly different results at higher energies. Nevertheless, during the last 50 years some important characteristics of spectra were established during intensive measurements with EAS surface detectors. For the list of detectors and their operational characteristics, see (Haungs et al., 2003). The most striking feature of the spectra is the approximately constant power index in whole examined energy range. The power index slightly changes from value $\gamma \sim -2.7$ to value $\gamma \sim -3.0$ at 3-4 PeV (the "knee" or also known as suppression of spectra) and it is another important and well established feature of the EAS spectra. Some authors (Nikolsky et al., 2000), (Nikolsky et al., 2003) claim that this "knee" is a feature of only the size spectra, reflecting some peculiarities of the EAS propagation and interaction in the atmosphere and the flux of the cosmic rays incident on the atmosphere can be described by a constant power index and that the CR origin is of extragalactic nature. In the paper (Stenkin, 2003), the "knee" of the EAS spectra is treated as consequence of the shower size reconstruction method only. He demonstrates that, the difference between pure electromagnetic showers and those having survived hadron "cores" can be the cause of the "knee." Another, very interesting approach is connected with the enigma of supernovae implosion and collapse. In (Plaga, 2002) the cannonball model of the supernovae explosion (Dar et al., 1999) was proposed as a source of the cosmic rays. The blobs of plasma with mass

the size of Earth are ejected from poles of supernovae at nearly light-speed. The population of such plasmoids filling the Galactic halo is responsible for the acceleration of the major part of the hadronic cosmic rays with energies up to another feature of all the particle spectra, the so called “ankle” occurring at $E > 10^{17}$ eV.

In contrast to these theories, the “standard” models of CR acceleration name the Supernovae remnants (SNR) as a major source of CR. The detected non-thermal radio emission from SNR, which led to the natural assumption of the presence of accelerated electrons, made SNR the main candidate engine for particle acceleration (Kayama et al., 1995). Recent CHANDRA very detailed measurements of the X-rays from SN 1006, (Long et al., 2003) imply a very large effective magnetic field of $100 \mu\text{G}$ in the Supernovae remnant. In the (Berezhko et al., 2003) the authors conclude that such a large field could be generated only due the nonlinear interactions of the accelerated protons and stripped heavier nuclei with self-generated Alfvén waves in a strong shock. Therefore, the SN 1006 data confirms the acceleration of the nuclear component at least up to several units of 10^{14} eV. Gamma-ray pulsars usually located near the SNR center are another candidate for cosmic ray acceleration (Bednarek et al., 2002). As mentioned in (Bhadra, 2003) pulsar accelerated cosmic rays are expected to have a very flat spectrum. Therefore, the impact of the nearest pulsar to energies higher than 10^{14} eV can be tremendous and can explain the fine structure of the energy spectrum, which may reflect acceleration of the specific groups of nuclei.

To investigate various scenarios of particle acceleration in SNR, we still have to use indirect information contained in CR spectra in the vicinity of Earth. As Galaxy magnetic fields cannot confine particles with such high energies, the extragalactic origin of the highest energy particles is widely accepted. The MAKET ANI installation, due to its modest size, is effectively collected cores of EAS initiated by primaries with energies up to several units of 10^{16} eV, therefore, we will constrain our analysis by the energy range $5 \cdot 10^{14} - 2 \cdot 3 \cdot 10^{16}$ eV – the so called “knee” region. Energy spectra of primary ions from $Z=1$ to $Z=26$ will provide valuable information on the validity of the standard model. Information from the EAS experiments does not provide enough clues for such “spectroscopy” of the “knee region”. Nevertheless, precise measurements of the electron and muon content, and implementation of the CORCIKA simulation code by the KASCADE experiment (Heck et al., 1998) as we have demonstrated in numerous papers (see for example (Chilingarian et al., 1999a), (Antoni et al., 2003a)), allows the classification of primaries according to 3 classes: “light”, “intermediate” and “heavy”. Using nonparametric multivariate methodology of data analysis ((Chilingarian, 1989), references on development and application of methods contained in (Chilingarian et al., 2003a), we solve the problem of the event-by-event-analysis of EAS data (Chilingarian et al., 1991), using Bayesian and Neural Network information technologies (Chilingarian, 1994, 1995), (Bishop, 1995).

At each stage of the analysis we estimate the value of the information content of the variables used for EAS classification and energy estimation and restrict the complexity of the physical inference according to this value. The MAKET-ANI experiment is located at 3200 m. above sea level on Mt. Aragats, In Armenia; the quality of reconstruction of the EAS size and shape are good enough and we can use them for the EAS classification shower size and shape parameters (the so called shower age). The distinctive information contained in distributions of these 2 parameters allows us to classify the EAS with high level of accuracy into 2 distinct groups: initiated by “light” or “heavy” nucleolus. In the KASCADE experiment (Antoni et al., 2003b), where the muon content of the EAS is measured in addition to shower electron size, and we can classify showers into 3 categories adding also the “intermediate” class.

COSMIC RAY ACCELERATION IN SUPERNOVAE EXPLOSIONS AND PROPAGATION IN THE INTERSTELLAR MEDIUM

The Power of Cosmic Ray (PCR) sources should be more than $\sim 10^{41}$ erg/sec to maintain the estimated cosmic ray energy density in the Galaxy. This value was obtained by multiplying the CR energy density in the Galaxy $\rho_{\text{CR}} \sim 10\text{-}12$ erg/cm³ by the Galaxy volume $V_G \sim 10^{67}$ cm³ and dividing by the particle mean escape time from the Galaxy $\tau_{\text{esc}} \sim 10^{14}$ sec. The kinetic energy of supernova ejecta, $W_{\text{SNR}} \sim 10^{52}$ erg and the frequency of the SN explosions in the Galaxy, $\text{freq} \sim 1$ in 20 years, lead to the CR luminosity of the same order of magnitude as if we assume that a few tens of percent of the ejecta kinetic energy is transformed to the CR energy.

The power law is rather satisfactory to describe the spectra from 10^{12} eV (far above solar modulation effects), up to several units of 10^{18} eV, where the Galaxy magnetic field of $\sim 3 \mu\text{G}$ cannot confine the particles anymore. At low energies up to 10^{14} eV the spectral indices of protons, carbon, oxygen and iron are very close to each other and equal to ~ -2.7 . The same index describes the spectra of

all the particles from 5×10^{14} up to $3-4 \times 10^{15}$ eV (the knee region), where the power index changes to ~ -3 , and returns to the value of -2.7 at several units of 10^{17} eV (the so called ankle region). The “classical explanation” of the changing behavior of the spectra consists of the existence of 3 distinct acceleration mechanisms: the first, usually connected with SNR shock acceleration, fades in the knee region; the second, due to unknown causes, is responsible for energies from the knee to the ankle region; and third, due to extragalactic sources, after the ankle.

Numerous papers are devoted to SNR-based acceleration. The obtained values of the spectra at the source obey the power law with index of $\gamma_s \sim (-2.0 - -2.1)$. Models of particle acceleration in the SNR can be compared with observations only if we account for the diffusion and escape of CRs from the Galaxy. Usually energy dependence of the escape time is also taken from the power law $-\tau_{esc} \propto E^{-\chi}$, and the relation between the spectra of CR in the source and the detected spectra takes the form $E^{-\gamma} \propto E^{-(\gamma_s + \chi)}$. Theoretical calculations of the diffusion coefficient are based on assumptions regarding the distribution of magnetic inhomogeneities in the Galaxy. There are 2 main distributions: “Kolmogorov Spectrum”, giving $\chi=0.33$ and “Kraichnan spectrum”, giving $\chi=0.5$. Measurements of the spectra of low energy isotopes (“radioactive clocks”) gives another value of $\chi=0.6$. This value, seems to be in perfect accordance with the observed spectra of $\propto E^{-2.7}$, but it addresses only the low energy particle data available from satellite and balloon isotope spectrometers. Additional measurements of isotope spectra at higher energies are needed. Since we cannot resolve the “all particle” spectrum, attempts are made to at least estimate the trend of the changing “mean mass”. The calculations of the average depth of the shower maximum, made using data measured by the fluorescence and Cherenkov detectors signal on “lightening” of mean mass just before the knee, and transition to heavies above the knee. This behavior could be explained by the influence of one or several of the nearest SNR, giving additional surplus flux added to the smeared superposition of thousands of Galaxy SNRs. If the knee feature is due only to numerous distant sources, the steepening of the spectra should be much smoother than detected. Attempts to find time-temporal coordinates of the SNR, which would explain the observed fine structure of the spectra, heavily depend on the adopted energy dependence on the diffusion coefficient. Authors of the recent estimates of the possible location of the Single Supernovae (SS) (Erlykin et al., 2003), proceeding from the “anomalous” diffusion introduced in (Lagutin, 2001), derive the following constraints for location and age of the SS - 300 – 350 pc from the Sun and 90 – 100 kyear old. They also adopted the energy dependence of the diffusion coefficient with $\chi=0.5$. Very Long Baseline interferometric measurements of the 100 Kyear old pulsar PSR656 + 14 (Brisken et al., 2003) locates the pulsar in the center of the SNR called Monogem Ring at 300 pc distance from the Sun. Therefore it was logical to assume that the Monogem Ring, the shell of debris from a supernova explosion, was the remnant of the blast that created the pulsar (Thorstett et al., 2003).

THE MAKET-ANI EXPERIMENT

The MAKET-ANI surface array (Chilingarian et al., 1999b) consists of 92 particle density detectors formed from plastic scintillators with thickness of 5 cm. Twenty four of them have area 0.09 m^2 and 68 area 1 m^2 . The central part consists of 73 scintillation detectors and is arranged in a rectangle of $85 \times 65 \text{ m}^2$. Two peripheral points at a distance of 95m and 65 m from the center of the installation, consist of 15 and 4 scintillations, respectively. In order to estimate the zenith and azimuthal angles, 19 detectors out of the 92 (each with area 1 m^2) are equipped with timing readouts to measure the timing of the appearance of the EAS front with an accuracy of $\sim 5 \text{ ns}$. The photomultiplier tubes (PM-49) of the detectors are placed in light-tight iron boxes. Logarithmic Analog to Digital Converters (ADC) and Constant Fraction discriminators (CFD) are assembled just above the photomultiplier tube (PM). The dynamic range of the registered particle number is $\sim 5 \cdot 10^3$.

Two types of detector triggers are used:

1. The hardware trigger: at least 7 of 11 central density detectors must be hit with more than 3 particles.
2. The timing trigger: at least 4 from 9 timing detectors, symmetrically arranged relative to the center, must be hit.

If the first two conditions are fulfilled in a time window of 20 μsec , then the event is stored. The trigger and data readout systems are according to CAMAC standard. Monte-Carlo calculations show that the this trigger system selects EAS with sizes $N_e > 5 \cdot 10^4$ and cores located within the rectangle of $40 \times 12 \text{ m}^2$ around the geometrical center of the installation.

The uncertainties of the reconstruction of the EAS parameters are as follows: shower size $\Delta N_e \sim 10\%$, the shower shape (age) parameter - $\Delta s \sim 0.06$. The accuracies of the EAS angle determination are $\Delta\theta \sim 1.5^\circ$ and $\Delta\phi < 5^\circ$.

In the period from 1998 – 2002, approximately 7,788,000 EASs were registered with effective registration time of about 24,000 hours. From these showers only $\sim 963,000$ events were selected for the spectra calculation. The selection criteria was to have more than 95% efficiency of registration, so we selected EAS core from the more compact area around the geometrical center of the MAKET detector, ensuring high efficiency of EAS registration. The following cuts were applied for the events selection: $N_e > 10^5$, $0.3 < s < 1.7$, $-24\text{m} < X_0 < 24\text{m}$, $-12\text{m} < Y_0 < 12\text{m}$, $\theta < 45^\circ$.

During multiyear measurements, the detecting channels were continuously monitored. Data on background cosmic ray spectra was collected for each detector. The slope of the spectra was used for detector calibration. The slope of background spectra is a very stable parameter and does not change even during very severe Forbush decreases, when the mean count rates can decrease as much as 30% (Chilingarian et al., 2003b). The detailed information about the MAKET-ANI detector operation during 1997-2003, including various comparisons and uniformity checks are summarized in (Hovsepyan et al., 2002, 2003).

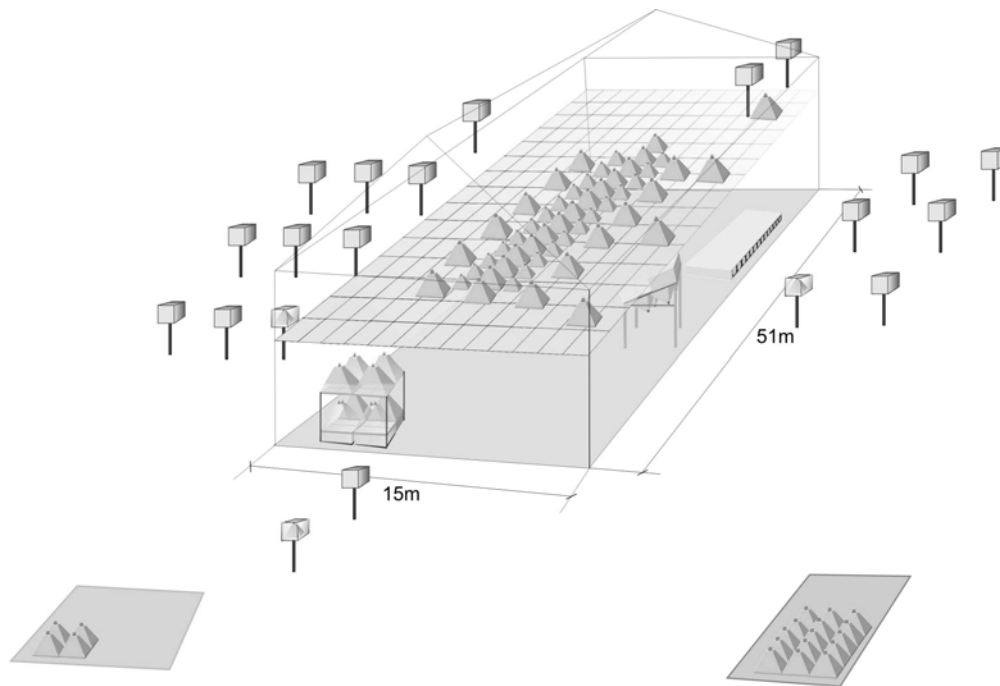


Figure 1 MAKET-ANI detector setup

SELECTION OF EAS PARAMETERS FOR CLASSIFICATION AND ESTIMATION

We are interested in choosing a combination of the EAS measured characteristics significantly differing from light and heavy initiated showers. The discriminative power of EAS characteristics were investigated using CORSIKA. (Heck et al., 1998) and MAKET-ANI response simulation codes (Hovsepyan, 2002). For comparison of EAS initiated by different primary ions a number of statistical methods were used, including one-dimensional statistical tests, correlation analysis and misclassification rates estimation by neural and Bayesian classifiers. Input parameters of the simulation program included particle type, energy, angles of incidence, as well as geographical coordinates and altitude of the MAKET-ANI detector. Energy and angular distributions taken reflects modern theoretical expectations. Due to the stochastic nature of particle propagation through the atmosphere the output parameters of simulation programs are random variables. We proceed according to the assumption of 2-way division

of all primary nucleolus, the so called, “light” and “heavy” mass groups. As representatives of the light group we will take the proton and He nucleus, for heavy group - Si and Fe nucleus will be the representatives. The intrinsic differences of the light and heavy ion cascades in the atmosphere make the distributions of EAS parameters different. We investigate if this difference is sufficient for reliable 2-way classification and take into consideration the way that the detector response smears it. Integrated over the entire energy range, the shower sizes of EAS initiated by heavy and light nuclei are also very similar. The only parameter showing significant difference between the two is the shower shape – age (s) parameter. Although the detector smears this difference, it remains significant enough, and as we will see further, the various correlations of this feature with shower size, make the pair of parameters (N_e , s) effective both for classification and energy estimation.

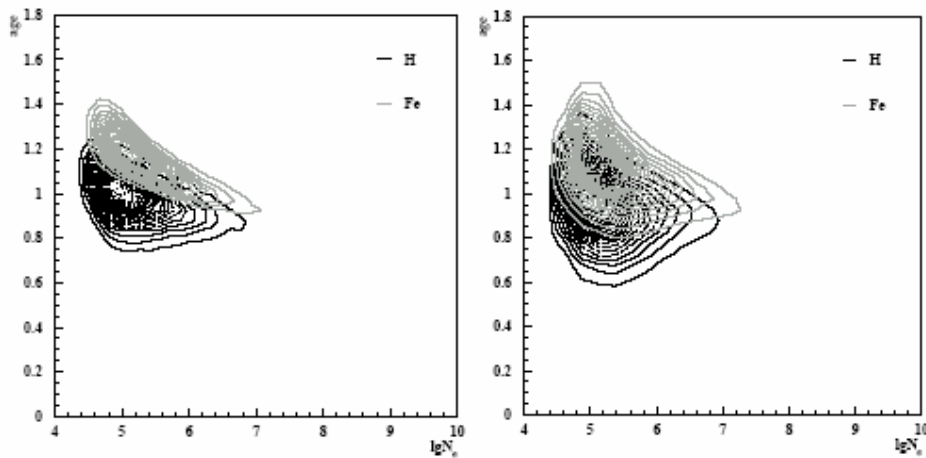


Figure 2 Scatter plot Shower Age versus Shower Size for simulated light and heavy primaries with (right) and without (left) incorporating of detector response.

The most direct estimates of the “discriminative power” of EAS characteristics are obtained by the classification of the samples using EAS simulations. Overlapping of the 2-dimensional distributions apparent from Figure 2 could be calculated numerically by the estimation of the misclassification rates from Bayesian or neural network classification of EAS initiated from the alternative groups of nuclei. Using only EAS electron characteristics, we cannot resolve nuclei with similar masses, such as p and He, or Fe and Si, therefore we join these nucleus in groups naming them “light” and “heavy”, thus restrict ourselves to the 2-way classification of the experimental data. Expected classification results posted in the Table 1 and

Table 2 demonstrate, that although detector smearing significantly enlarges misclassification rates, nevertheless >70% correct classification is very encouraging and the $N_e - s$ pairs as measured by the MAKET ANI detector provide enough information for the 2-way classification. We also want to point out the good agreement between results obtained by using 2 completely different methods of classification: Bayesian classification with nonparametric estimation of multivariate probability density function and Neural Network classification using stochastic net training methodologies.

Table 1 Neural classification into two classes using H+He and Si+Fe events without and with detector response

	Without detector response		With detector response	
	Light	Heavy	Light	Heavy
Light	0.925	0.075	0.720	0.280
Heavy	0.045	0.955	0.240	0.760

Table 2 Bayesian classification into two classes using H&He and Si&Fe events without and with detector response.

	Without detector response		With detector response	
	Light	Heavy	Light	Heavy
Light	0.938	0.062	0.712	0.288
Heavy	0.043	0.957	0.237	0.763

DATA CLASSIFICATION INTO LIGHT AND HEAVY GROUPS OF NUCLEI, PURIFICATION OF SELECTED GROUPS OF NUCLEI

According to the results from the previous section we use 2 “training samples” of “light” and “heavy” nuclei initiated N_e -s pairs, generated by the CORSIKA code including the MAKET-ANI response function. Before Neural classification of the MAKET-ANI data we investigate the expected purity¹ and efficiency² of our data analysis procedures. From Table 3 we can see that efficiency of classification, i.e. correct identification of nuclei from light and heavy groups is above 70%, the “intermediate” Oxygen nuclei are distributed approximately equally among 2 groups. To obtain purity estimates we assume the so called “normal” primary composition: 30% H, 24% He, 17% O, 17.5% Si and 11.5% Fe. Table 2 demonstrates that the purity of the light group is above 70% and the purity of the heavy group is below 50% with large contamination of the Oxygen and light nuclei.

Table 3 Efficiency of the neural classification of EAS initiated by different primaries into two mass groups

	light	Heavy
H	0.720	0.280
He	0.691	0.309
O	0.453	0.547
Si	0.352	0.648
Fe	0.240	0.760

Table 4 Purity of the classification of different nuclei in light and heavy groups

	H	He	O	Si	Fe
Light	0.407	0.298	0.137	0.111	0.047
heavy	0.162	0.167	0.208	0.255	0.208

To enlarge the purity of the heavy nuclei group we introduce the purification procedure described in (Antoni et al., 2003a), enlarging the purity of each nuclear group at the cost of decreasing the efficiency. The purification of the selected "light" and "heavy" groups was done by selecting the appropriate domain in the entire range of the network output. The feed-forward Neural Network (NN) performs a nonlinear mapping of the multidimensional characteristics of the EAS to the real number interval [0,1], called the output of the NN. Figure 3 shows the network output histogram. The network was trained to shift the "heavy" group to the right and the "light" group to the left of the histogram. The 0.5 point of the NN output is the so called decision point. The particular class assignments for the two-way classification are the subintervals [(0.0,0.5) and (0.5,1.0)] for the "light" and "heavy" class

¹ purity: fraction of true classified events in an actual number of events assigned to a given class

² efficiency: fraction of true classified events in total number of events of a given class

respectively. If the neural network is satisfactorily trained to have generalization capabilities, the output distributions for the different classes will overlap at the subinterval boundaries. Therefore, by shrinking the subintervals, i.e. moving the interval boundary to the left and right of the decision point 0.5, it is possible to remove a large portion of the misclassified events. Of course, simultaneously we lose parts of the true-classified events, i.e., decrease the efficiency. Thus, instead of one decision point in the middle of the NN output interval, we will have two "decision intervals" for accepting "light" and "heavy" nuclei, and a third interval in between where we reject the classification. Figure 3 demonstrates this "purification" procedure.

Figure 4 shows the results of the purification. The values next to the symbols indicate the selected decision interval used for obtaining the particular purity-efficiency relation. For example, if we select the $[(0.0,0.3)$ and $(0.7,1.0)]$ intervals for classification of the "light" and "heavy" nuclei, we obtain 96% purity and 56% efficiency for the "light" class; 78% purity and 55% efficiency for the "heavy" class. Therefore, we can enhance the purity of the light nuclei up to 95% and the purity of the heavy nuclei up to 80%, while still holding the efficiency above 50%. The purity and the efficiencies are obtained by classifying 35000 light (H,He) and 17000 heavy (Si,Fe) control events, which are not used for the training of the neural network. Artificially high purity for both classes is achieved from using this method as demonstrated in Table 4, since the intermediate nuclei (simulated oxygen initiated EAS) were not included in the analysis. More realistic purity and efficiency estimates are apparent from Table 5 and Table 6, where we include also the Oxygen nuclei.

Table 5 Efficiency of the neural classification of EAS initiated by different primaries into two mass groups (purification intervals $[0.,0.3)$ and $(0.7,1.]$).

	light	Heavy
H	0.567	0.095
He	0.475	0.135
O	0.252	0.303
Si	0.176	0.393
Fe	0.099	0.561

Table 6 Purity of the classification of different nuclei in light and heavy mass groups (purification $[0.,0.3)$ and $(0.7,1.]$).

	H	He	O	Si	Fe
Light	0.459	0.310	0.115	0.084	0.032
heavy	0.115	0.131	0.207	0.278	0.268

As we can see from Table 6 the purity of the light group increases from 70 to 77% and for the heavy ones from 46 to 55%, we need to keep in mind that approximately 20% of the heavy group are due to showers initiated by O nuclei. The purification allows us to significantly increase the purity of 2 alternative samples and we can, therefore, estimate the energy spectra of light and heavy groups. Of course, first we should describe the energy estimation procedures used.

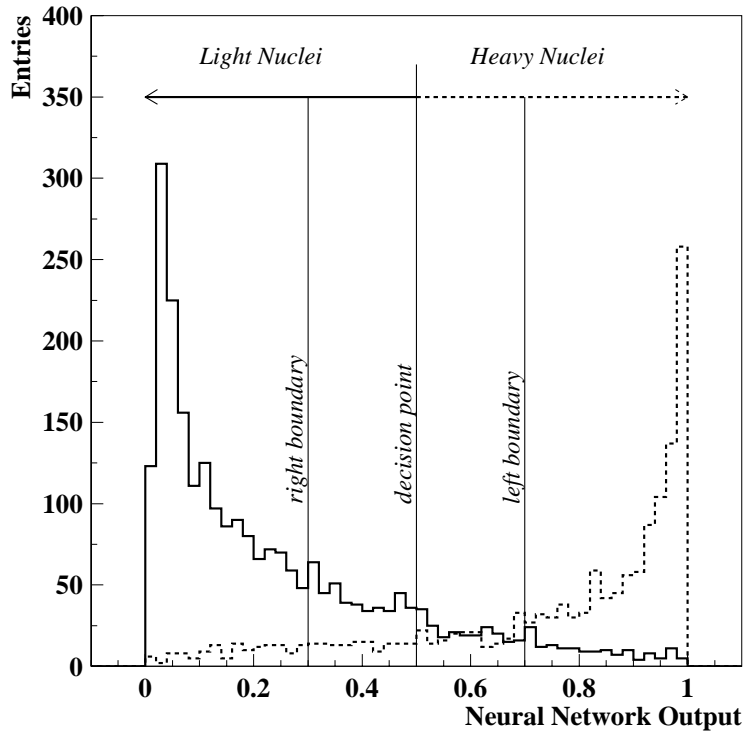


Figure 3 Output of the Neural Network (NN) trained to distinguish light and heavy nuclei.

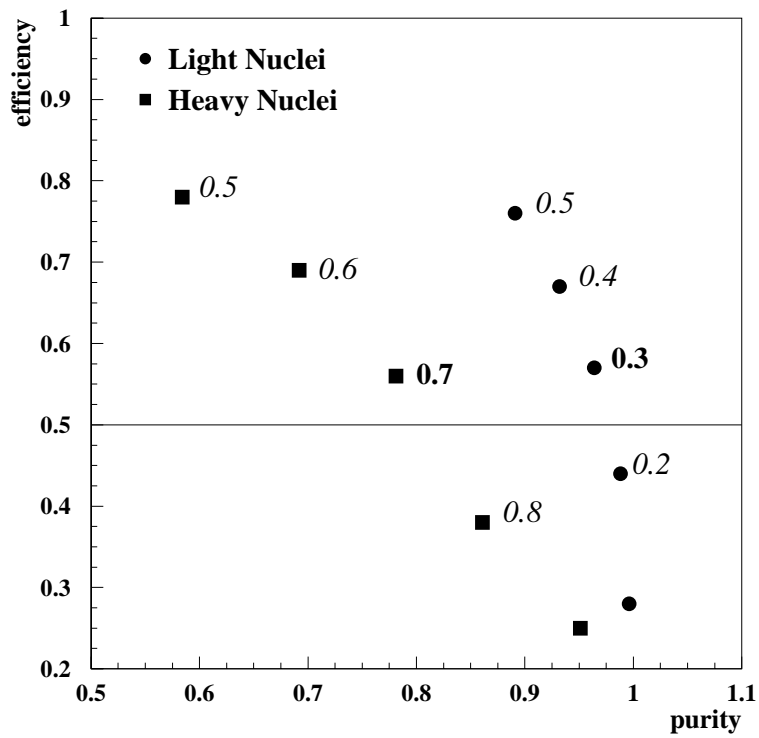


Figure 4 Purity – Efficiency plots obtained by shifting the NN decision boundaries

ESTIMATION OF THE PRIMARY ENERGY OF DIFFERENT GROUPS OF NUCLEI

The primary energy of each shower was obtained by neural network estimators separately for the light and heavy nuclei induced events, exploiting very large correlation of shower size N_e with primary energy and different correlations between primary energy and shower shape in light and heavy nuclei groups. In Figure 5 relative errors of energy estimation for 10 energy intervals are posted. The bias of the energy estimation, displayed does not exceed the 5% for the light group (left) in the whole energy range except the lowest energies. For the heavy group of nuclei the estimation bias in the energy range of 10^{15} — 10^{16} eV is not larger than 5%, nevertheless, one can observe some overestimation for low and high energy regions. The energy resolution for heavy group of nuclei is significantly better (MSD ~ 20%) as compared to the light group of nuclei (MSD ~ 30%) due to the smaller fluctuations of heavy initiated EAS size and shape. Also, accuracy of the energy estimation is enhancing with enlarging primary energy.

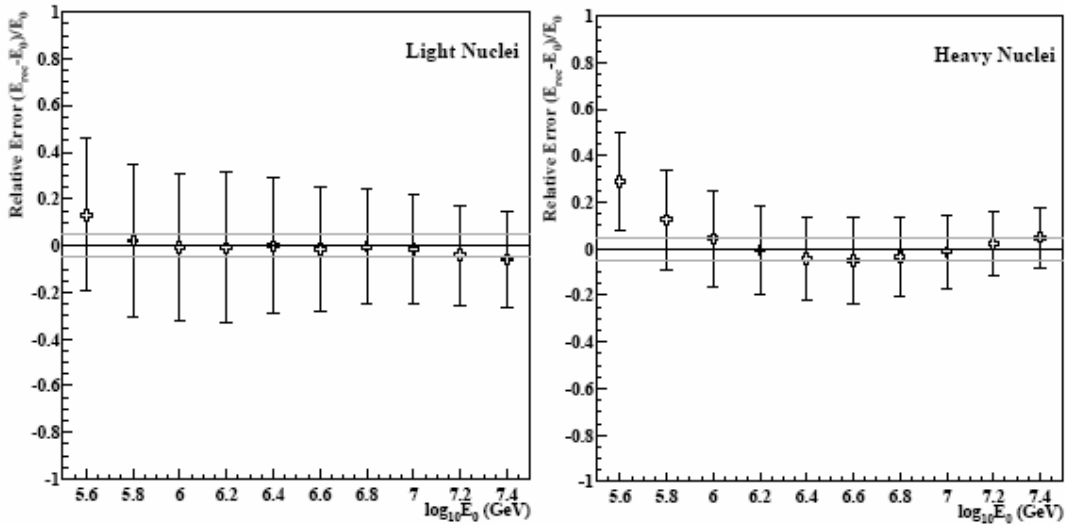


Figure 5 The relative errors of energy estimates for 10 energy intervals of light and heavy groups.

the 2 horizontal lines around the 0-line outline the $\pm 5\%$ error corridor. Error bars are correspondent to Root Mean Square (RMS) deviation.

ENERGY SPECTRA

Figure 6, adopted from (Haungs et al., 2003), shows the energy spectrum measured by different detectors exploiting various experimental techniques and the energy reconstruction methods. Energy estimation for all experiments was made using Monte Carlo simulations with different numerical algorithms. Despite considerable differences in experimental techniques and different EAS components (shower shape and electron size parameters, muons, Cherenkov light) used for the energy estimation, and the differences in systematic errors (usually not reported in publications), almost all spectra are in rather good agreement if we assume an energy estimation accuracy of $\sim 20\%$. Only at energies higher than the knee feature does the spectra disagree, probably because of the saturation effects in the scintillators in some experiments. All particle spectra and mean logarithmic mass, in many cases presented as an outcome of the EAS experiment, are not very informative. We never know which combination of primaries constitutes the mean and which groups of primaries are responsible for the knee. The best solution will be to separate different groups of nuclei and reconstruct energy spectra to determine the spectral knees of different nuclei at different positions. This program was partly fulfilled with the data from the MAKET-ANI experiment. After checking for the purity and the efficiency of each of the nearly 1 million showers registered by the MAKET-ANI installation in 1999-2002, shower sizes greater than 10^5 were classified according to the techniques described in (Chilingarian et al., 1991), (Antoni et al., 2003a). The energy of the classified particles in 2 distinct classes of showers was estimated for each group separately, using again the CORSIKA simulations and neural estimation techniques. Using the EAS characteristics of Shower Size (N_e) and Shape (s), we plot the obtained energy spectra of the "light" and "heavy" mass groups, see Figure 1.

The spectrum of the "light" group shows a "knee" in the region of $3-4 \cdot 10^{15}$ eV. The "knee" feature is not observed for the spectrum of the "heavy" component, at least not up to energies of 10^{16} eV. The number of "light" and "heavy" nuclei at $\sim 10^{15}$ eV is approximately equal and the number of "heavy" nuclei gets

larger at energies greater than the "knee" energy. The "purified" spectrum, see Figure 8, show lower flux intensities for both classes of particles due to the lower efficiency. The "knee" position shifts to lower energies because after purification the proportion of protons is enlarged. In addition, the slope of the spectrum (spectral index) of the "purified" light component becomes steeper, -2.63 , compared to -2.54 before purification. Both results are consistent with the rigidity dependent acceleration and consequent fading of the proton flux at high energies.

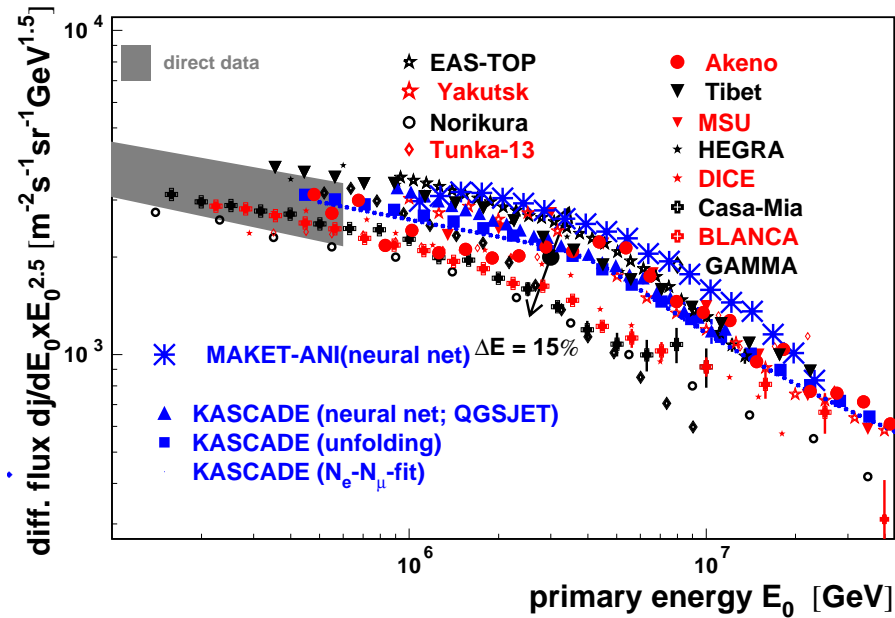


Figure 6 Summary of the all particle spectra from 18 different experiments

Another important feature of the obtained spectra is the very large difference between spectral indices before and after the "knee": $\Delta\gamma(light) = \gamma_2 - \gamma_1 \sim 0.9$. It is well known that the same parameter for the all-particle spectra is $\Delta\gamma(all - particle) \sim 0.3$, (Haungs et al., 2003). Erlykin and Wolfendale, in their simulations, were not able to reproduce the actual shape of the all-particle spectrum by averaging the proton and nuclei fluxes produced by nearly 50,000 distant supernovae in our Galaxy (Erlykin et al., 2001). Therefore, they propose that the nearby young supernova (< 500 pc and < 110 kyr), is responsible for the approximately 60% of the detected cosmic ray flux in the vicinity of earth (Erlykin et al., 2003). The very large difference of the spectral indices before and after the knee of the "light" component (~ 0.9) confirms the Erlykin and Wolfendales proposal regarding the huge impact of the nearest supernova on the cosmic ray flux in the vicinity of earth. It suggests the necessity to make detailed calculations of the influence of the nearest supernova on the detected cosmic ray fluxes, i.e., to obtain the partial spectra of the nuclei accelerated by the single source (for a candidate of such source see (Thorsett et al., 2001)).

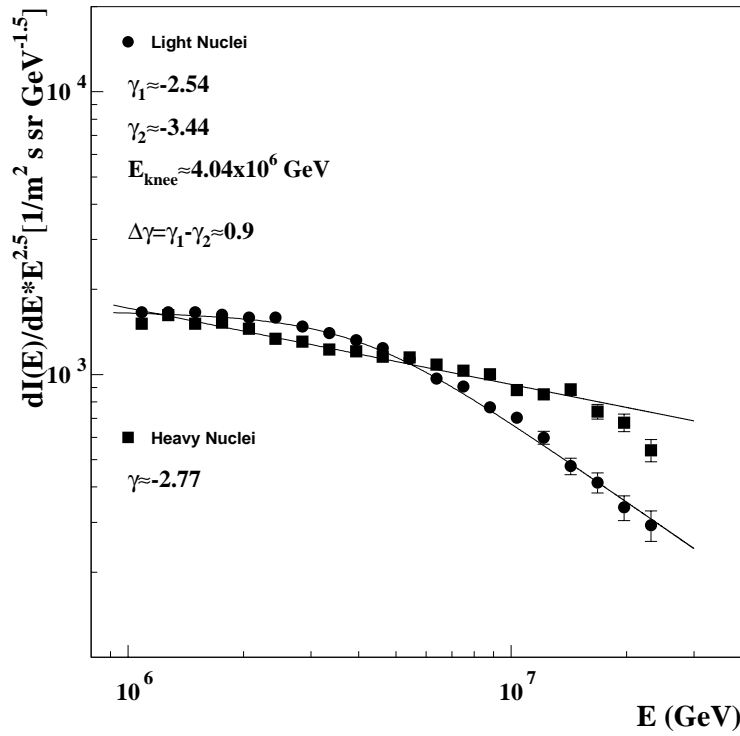


Figure 7 Energy spectra of light and heavy nuclei obtained by neural classification and energy estimation. EAS characteristics used : Shower Size and Shape (Age).

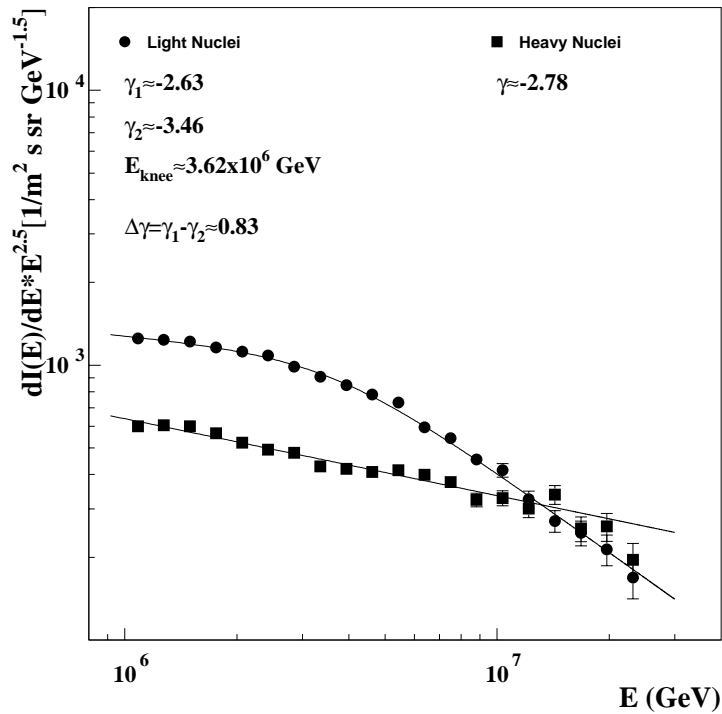


Figure 8 Energy spectra of light and heavy nuclei obtained by neural classification and energy estimation. The same as in Figure 7 but obtained with purified light and heavy data samples. Purification intervals: [0.,0.3) and (0.7,1.].

WHAT WE CAN LEARN FROM SOLAR ACCELERATORS

Starting from the 70s, with the launch of particle spectrometers, began the continuous monitoring of the low and medium energy cosmic rays in space. Time histories of the simultaneously detected X-rays, gamma-rays, electrons, and ions of different energy and charge, combined with the detection of the developing flares and Coronal Mass Ejections (CME) using coronagraphs, helped to create a comprehensive picture of the major solar events, accelerating protons to high energies, the so called, Solar Energetic Proton (SEP) events (Reames, 1999). SEP events include also highest energy ions and accompanying protons, giving rise to Ground Level Enhancements (GLE) and additional fluxes of secondary cosmic rays (mostly neutrons and muons), detected by the world-wide network of the Neutron Monitors and Muon Telescopes. "New Instruments on WIND and ACE satellites operating during the 23-rd solar cycle, with geometry factors ~100 times larger than those of the previous cycle, have yielded unprecedented observations of temporal evolution in composition and spectra over a wide range of energies and species" (Tylka et al., 2001b). Multiwavelength measurements from very sensitive X-ray detectors, high resolution imaging coronagraphs and radiotelescopes now reveal the location and characteristics of the natural accelerators at the Sun and in the interplanetary space in much more detail.

Impulsive flare events are believed to accelerate electrons and ions in large structures originating in the magnetic reconfiguration regions. After discovery of the above-the-loop-top hard X-ray source (Masuda et al., 2001), with the Yohkoh/HXT (Kosugi et al., 1991), it became apparent that particles are accelerated by the dynamic electromagnetic forces during the reconfiguration of the magnetic fields (Ashwanden et al., 1996). The most probable acceleration mechanism is the stochastic acceleration, allowing detectable intensities of nonthermal X-ray radiation from locally trapped electrons. Direct hard X-ray detection, as well as application of the time-of-flight technique to the electrons traveling from acceleration site to the chromosphere reveals that the location of the acceleration region is 5,000 – 35,000 km above the top of the soft X-ray-bright flare loop (Ashwanden, 2002). The natural assumption that positively charged protons and ions will be accelerated with the same mechanisms as the electrons is proven by the registration of the lined gamma radiation in coherence with hard X-ray radiation. The time sequence of the bremsstrahlung radiation peaks produced by accelerated electron beams, interlaced by the nuclear de-excitation lines produced by proton and ion bombarded chromosphere, clearly demonstrate, that ions and electrons are accelerated in the same region and nearly simultaneously. The efficiency of the stochastic acceleration of ions via the mutual wave-particle interactions depends on the relation between the frequencies of the resonant waves (Alfvén waves, magnetosonic waves, sound waves) and ion gyrofrequency. Alfvén waves, if fast enough (~2000 km/sec), can accelerate 20 KeV protons up to GeV energies during time scales of 1-10 sec. (Barbosa, 1979), (Miller et al., 1990).

Gradual events are associated with CME development in corona and in interplanetary space. CME driven shock should be fast enough (> 500 km/sec, Reames, 1999) to produce SEP events. Shock acceleration is believed to be one of the major mechanisms in the Universe for accelerating particles to highest energies. Multiple traversals of shock are required for the acceleration of solar ions up to MeV energies. Ambient magnetic turbulence is not sufficient for scattering and trapping ions with such energies. Self-generated Alfvén waves effectively scatter energetic ions, providing their trapping near the shock and, therefore, increasing their energy. Maximum attainable energy of accelerated ions is proportional to the rate of re-crosses of the shock. This rate, in turn, is proportional to the particle trapping time. "As trapping increases for particles of one rigidity, they are more likely to be accelerated to a higher rigidity, where they again stream out and produce resonant waves, etc" (Reames, 2000). Numerical calculations and Monte Carlo simulation prove that solar protons could be accelerated up to energies of 100 GeV during propagation of the CME in middle and high corona (Miller et al., 1990). The same authors examining the 1982 June 3 flare, mention that protons were accelerated within 16 seconds from 30 MeV to ~1 GeV. Krucker and Lin, (Krucker et al., 2000), based on the data from WIND/SST instrument (Lin et al., 1995), conclude that protons at energies up to 6 MeV are injected simultaneously at heights $\leq 10 R_{\odot}$. The maximum energy attainable by the shock acceleration depends on the shock speed and the height of the shock starts in the corona. Shock waves as fast as $\sim 1500 \text{ km sec}^{-1}$ starting below $\sim 5 R_{\odot}$ can accelerate ions up to 10-30 GeV (Tulka et al., 2001c), (Tulka et al., 2001a). Study of the association between SEP events and CME (Gopalswamy et al., 2002) proves that CME interaction is important for high energy SEP production. For most of the SEP events detected in 1997-2001 the primary, fast CME overtakes one or more slower CMEs within a heliocentric distance of $\sim 20 R_{\odot}$. The summary of the present knowledge on particle acceleration by various mechanisms at the Sun and in the interplanetary space can be summarized as follows:

- Electron Accelerators also accelerate protons and heavier ions, acceleration sites are very close in space and time;
- Particle acceleration is much more effective when several shocks are present in the interplanetary space.
- The “magnetic bottle” structures formed by interacting shocks are major sites for reacceleration of particles primarily accelerated by “impulse” and “gradual” mechanisms;
- Maximal attainable energy of particle accelerators is proportional to the particle charge;
- Moving Shock is carrying bulk of particles;
- Maximal attainable energy of the particle changes from event to event and depends on the total energy of the solar blast, speed of the shock wave, and the time-temporal history of the solar flare. (Positions of the Spectral “knees” change from 10 MeV to several GeV).
- For detection of charged particles on the Earth, the shock should intercept observers magnetic tube;
- The streaming limit controls the transport of particles

The rigidity dependent maximal acceleration energy in solar Energetic Events (SEP), which occurred during the current 23rd solar cycle, is apparent from Figure 9. Again, as with galactic cosmic rays, we see very sharp knee for the light nuclei group, namely protons, and no knee for heavy nuclei group, namely iron.

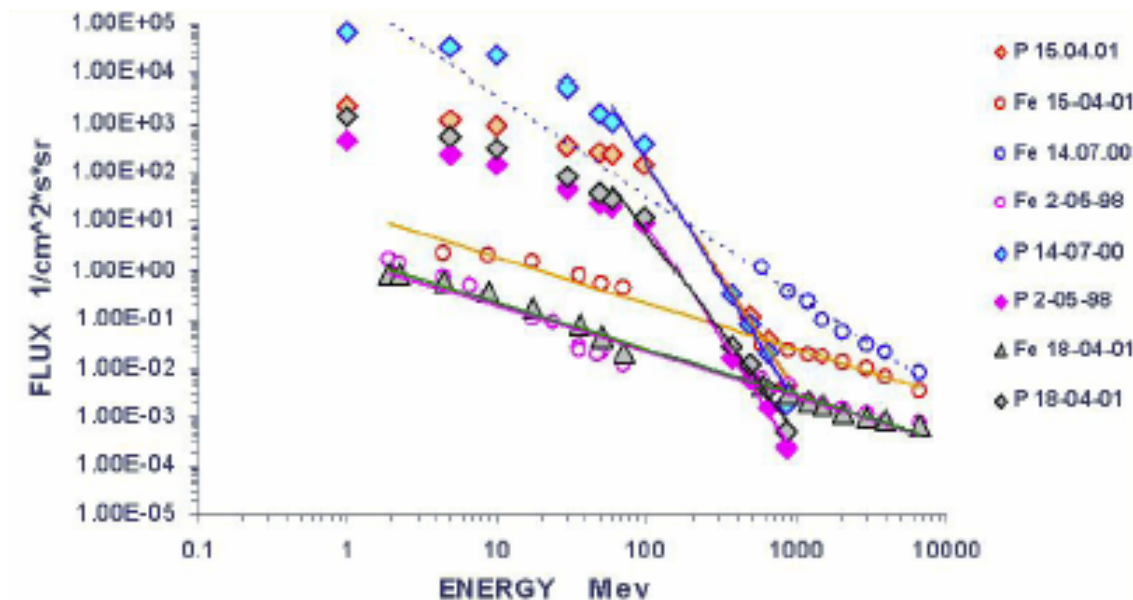


Figure 9 The energy spectra of protons and Fe ions registered by space-born detectors during an SEP event of 23-rd solar cycle.

The most famous, so called Bastille day SEP from 14 July 2000 event, as you can see from Figure 9 and from (Tulka et al., 2001a) demonstrates the remarkable exactness of the knee positions according to accelerated ion charge: proton knee is at ~20 MeV, He knee at ~40 MeV and Carbon knee at ~100 MeV. Carbon charge is equal to 5, and one should note that the temperature at and near the Sun is not high enough to fully strip the carbon ions, such as happens at Supernova explosion sites.

DISCUSSION AND CONCLUSIONS

Recent unprecedented detailed observations of the nonthermal X-ray radiation from SN 1006 made by CHANDRA (Longet et al., 2003), point very definitely at the SNR as the host of the hadron accelerators providing energy at least up to several units of 10^{14} eV. Observations of the wind synchrotron nebulae around pulsars in the vicinity of the SNR center reveals another accelerator site, e.g. the termination shock, at which the relativistic shock from the pulsars wind is forced to join the slower expansion of the outer nebula (Gaensler et al., 2003).

The Single Source, or Single Supernovae (SS) model of Erlykin and Wolfendale (Erlykin et al., 1997), (Erlykin et al., 1998), also attracts huge support by the discovery of the nearest pulsar, located at the space-temporal distance in remarkable concordance with SS model expectations (Thorsett et al., 2001).

The recent results, which came forth from the MAKET-ANI experiment, confirm the SNR and SS models of Cosmic Ray Origin. The very sharp knee of the energy spectrum of the light mass group suggests accepting the SS hypothesis, because it is highly improbable that a Galaxy ensemble of distant Supernovae, with a variety of explosion energies, shock wave speeds, distances and explosion times, will provide a sharp knee feature. Instead we should expect rather smooth depletion of the light mass group flux if the latter hypothesis were true.

The knee of the light mass group and the absence of knee in the heavy mass group up to at least 10 PeV also confirms the hypothesis of rigidity dependent maximal energy of SNR accelerators. Experimental evidence could be summarized in the following statements:

- The energy spectrum of the "heavy" mass group of cosmic rays shows no "knee" in the energy interval of 10^{15} - 10^{16} eV.
- The energy spectrum of the "light" mass group of nuclei shows a very sharp "knee" $\Delta\gamma \sim 0.9$ compared to $\Delta\gamma \sim 0.3$ for the all-particles energy spectra..

And finally we conclude that:

- The SNR acceleration model is supported by the MAKET-ANI data on partial energy spectra;
- Our conclusions on rigidity dependant acceleration are consistent with the evidence we saw recently about how the solar accelerators work. The recently proposed mechanisms of particle acceleration in the SN1006 (Berezhko et al., 2003) is fully consistent with the mechanisms of solar particle acceleration by CME driven shocks, of course, at much lower particle energy scales.
- The time history of the cosmic ray intensity (Schlickeiser et al., 2002), suggests 50% enhancement of the CR flux integrated over the last 400,000 years, compared to all available time record of 10^9 years. It is also consistent with the nearby SS model.

ACKNOWLEDGMENTS

We thank the ANI collaboration members for their fruitful cooperation over many years and A.Haungs, H.Rebel and M.Roth for cooperation in development of multivariate methods of data analysis for KASCADE experiment and for kind permission to use Figure 6.

BIBLIOGRAPHY

- Adams J., Bashindzhagyan G., et.al.(2001), *Advances in Space Research*, **27**, No. 4, pp. 829-833
- Antoni T., et al., (KASCADE Collaboration), (2003a), *Astroparticle Physics* **19**, 715–728
- Antoni T., et al., (KASCADE Collaboration), (2003b), submitted to NIMA.
- Aschwanden M.J., Wills, M.J., et al., (1996), *ApJ* **468**, 398.
- Aschwanden M.J. (2002), *Space Science Reviews*, **101**, N 1,2.
- Bednarek W., Protheroe R.J. (2002), *Astroparticle Physics* **16**, 397.
- Berezhko E.G., Ksenofontov L.T., Volk H.J., (2003), *A&A*, **412**, 11.
- Bhadra A. (2003) *Proc. 28th Int. Cosmic Ray Conf. (Tsukuba)*, 303.
- Bishop C. M.: *Neural Networks for Pattern Recognition*. Oxford Univ. Press, New-York, 1995.
- Brisken, W. F., Thorsett, S. E., Golden, A., & Goss, W. M. 2003, *ApJ*, **593**, L89.
- Chilingarian A.A., (1989), *Computer Physics Communications*, **54**, 31.
- Chilingarian A.A., Zazyan H.Z. (1991), *IL Nuovo Cimento* **14C**(6), 555.
- Chilingaryan A. A. (1994), *Neurocomputing*, **6**, 497.
- Chilingarian A. A. (1995), *Pattern Recognition Letters*, **16**, 333-338.
- Chilingarian A.A. for the KASCADE collaboration et.al., (1997), In *Proceedings of 28-th ICRC, Durban, 1997*, v. , p.105.
- Chilingarian A. A.: *Analysis and Nonparametric Inference in High Energy Physics and Astroparticle Physics*, 1998. Program Package ANI, (Users Manual, unpublished) <http://crdlx5.yerphi.am/proj/ani>
- Chilingarian A.A., Roth M. and A.Vardanyan for the KASCADE collaboration, (1999a), *Journal of Physics G*, **75A**, 302.
- Chilingarian A., Gharagyozyan G., et.al.,(1999b), in *Proc. Of the Workshop ANI 99*, Ed. Chilingarian , Haungs,.Rebel, Zzazyan, Nor Amberd, 1999, FZK preprint 6472.
- Chilingarian A.A., Vardanyan A.A. (2003a), *Nuclear Instruments & Methods*, **502/2-3**, p 787.

Dar A., Plaga R., (1999), *A and A*, **349**, 259.
Gopalswamy N., Yashiro S., et.al, (2002), *ApJ* **572**, L103
Haungs A., Rebel H., and Roth M., (2003), *Rep. Prog. Phys.* **66**, 1145–1206.
Heck D. et.al., 1998, FZKA 6019, Forschungszentrum Karlsruhe
Hovsepyan G.G, (2002), ANI collaboration report N 2,
http://crdlx5.yerphi.am/ani/ani_collab.html
Kosugi, T., Makishima, et.al., (1991), *Solar Phys.*, **136**, 17.
Koyama K., Petre R., et.al.(1995), *Nature* **378**, 1306.
Krucker S., Lin R.P., (2000), *AJ*, **542**, L61.
Lagutin A.A., (2001), in *Proc. 27-th ICRC, Hamburg, 2001*, v. **5**, p. 1900.
Lin R.P., et.al.,(1995), *Sol.Phys.*, **71**,125.
Long K.S., Reynolds S.P., Raymond J.C. et al., (2003) *ApJ*, **586**,1162
Masuda S., Kosugi T., et.al., (1994), *Nature*, **371**, 495.
Hovsepyan G., Melkumyan L.G. et al. (2003), Ani Collaboration report N 6, YerPhi Preprint 1587/08
Miller J.A., Guessoum N., Ramaty R.(1990), *AJ*, **361**, 701.
Nikolsky S.I., Romakhin V.A., (2000), *Phys.Atom.Nucl.*, **63(10)**, 1799.
Nikolsy S.I., Sinitsyna V.G., in *Proc. 28-th ICRC, Tsucuba, 2003*, p.2007-2010.
Plaga R., (2002), *New Astron.* **7**, 317.
Reames D.V., (1999), *Space Sci. Rev.*, **90**, 413.
Reames D.V. (2000), SEPs: Space Weather Hazard in Interplanetary Space, in *Space Weather*, ed. By Schlickeiser R., (2002), *Cosmic Ray Astrophysics*, Springer, Berlin, Heidelberg, New-York, Tokyo, p.69.
Y.Stenkin, (2003), *Mod. Phys. Lett. A*, **18(18)**,1225-1234
Thorsett, S. E., Benjamin, R. A., Brisken, W. F., Golden, A., & Goss, W. M.
2003, *ApJ*, **592**, L71
Tylka A.J., Cohen C.M.S., et al, in *Proc. 27 ICRC*, **8**, 3189, Hamburg, 2001a.
Tylka A.J., Dietrich W.F., Lopate C., Reames D.V., in *Proc. 27 ICRC, Hamburg, 2001b*.
Tylka A.J., AGU publication N 2000JA004028, 2001c
Erlykin A.D., Wolfendale E.W., (1997), *J.Phys.G*: , **23**, 979.
Erlykin A.D., Wolfendale E.W., (1998), *Astropart. Phys.* **8**, 265.
Erlykin, A. D., and Wolfendale E. W. (2001), *J. Phys.G*, **27**, 941.
Erlykin A.D., Wolfendale E.W., (2003), in *Proc. 28-th ICRC, Tsucuba, 2003*, p.2349-2052.